Genetically enhancing mitochondrial antioxidant activity improves muscle function in aging

Alisa Umanskaya[a,1], Gaetano Santulli[a,1], Wenjun Xie[a,1], Daniel C. Andersson[a], Steven R. Reiken[a], and Andrew R. Marks[a,b,2]

[a]Department of Physiology and Cellular Biophysics, The Clyde and Helen Wu Center for Molecular Cardiology, Columbia University College of Physicians and Surgeons, New York, NY 10032; and [b]Department of Medicine, Columbia University College of Physicians and Surgeons, New York, NY 10032

Edited by Eric N. Olson, University of Texas Southwestern Medical Center, Dallas, TX, and approved September 15, 2014 (received for review July 7, 2014)

Age-related skeletal muscle dysfunction is a leading cause of morbidity that affects up to half the population aged 80 or greater. Here we tested the effects of increased mitochondrial antioxidant activity on age-dependent skeletal muscle dysfunction using transgenic mice with targeted overexpression of the human catalase gene to mitochondria (MCat mice). Aged MCat mice exhibited improved voluntary exercise, increased skeletal muscle specific force and tetanic Ca^{2+} transients, decreased intracellular Ca^{2+} leak and increased sarcoplasmic reticulum (SR) Ca^{2+} load compared with age-matched wild type (WT) littermates. Furthermore, ryanodine receptor 1 (the sarcoplasmic reticulum Ca^{2+} release channel required for skeletal muscle contraction; RyR1) from aged MCat mice was less oxidized, depleted of the channel stabilizing subunit, calstabin1, and displayed increased single channel open probability (P_o). Overall, these data indicate a direct role for mitochondrial free radicals in promoting the pathological intracellular Ca^{2+} leak that underlies age-dependent loss of skeletal muscle function. This study harbors implications for the development of novel therapeutic strategies, including mitochondria-targeted antioxidants for treatment of mitochondrial myopathies and other healthspan-limiting disorders.

aging | skeletal muscle | exercise capacity | muscle weakness | oxidation

Age-dependent muscle weakness is a leading cause of morbidity due to frailty, loss of independence, and physical disability that is associated with increased risk of falls and fractures (1, 2). In geriatric populations age-dependent muscle weakness, characterized both by loss of lean muscle mass (sarcopenia) and reduced skeletal muscle function (3–5), has been estimated to affect 30–50% of 80-y-olds (1, 2, 4).

The 'free radical theory' of aging, first proposed in 1956 by Harman (6), states that an underlying mechanism of age-dependent pathology is the accumulation of partially reduced forms of oxygen (7, 8), collectively known as reactive oxygen species (ROS). Mitochondria are a major source of cellular ROS (7, 9) and have been proposed to play a key role in age-dependent loss of skeletal muscle function (3, 7, 10), likely through the production of oxidative damage (11, 12). However, the molecular mechanisms underlying this process have not been fully determined.

Skeletal muscle contraction is dependent upon release of intracellular Ca^{2+} via the sarcoplasmic reticulum (SR) Ca^{2+} release channel, ryanodine receptor 1 (RyR1). Following membrane depolarization, voltage-sensing Ca^{2+} channels in the transverse tubules (Cav1.1) activate RyR1 and the ensuing rise in cytoplasmic [Ca^{2+}] causes muscle contraction via the actin-myosin cross bridge cycle (13). The RyR1 is a homotetrameric protein complex composed of four monomers, kinases, a phosphatase (PP1), phosphodiesterase (PDE4D3), calmodulin, and the RyR1 channel-stabilizing subunit calstabin1 (FK506 binding protein 12, FKBP12) (14). Post-translational modifications of the channel, including oxidation, cysteine-nitrosylation, and cAMP-dependent protein kinase A-mediated phosphorylation have been linked to impaired Ca^{2+} handling and perturbed contractility in chronic muscle fatigue, heart failure and muscular dystrophy (13–15). Furthermore, we have recently reported that both oxidation of RyR1 and the subsequent intracellular Ca^{2+} leak underlie the age-dependent reduction in skeletal muscle specific force (10). Acute induction of RyR1-mediated SR Ca^{2+} leak with rapamycin, which competes the channel-stabilizing subunit, calstabin1, off from RyR1 (14, 16), resulted in defective mitochondrial function associated with elevated free radical production (10). However, the role of mitochondrial ROS in age-dependent reduction in skeletal muscle function and exercise capacity has not been elucidated.

Recently, there have been numerous efforts to study mitochondria-derived free radicals in health and lifespan by experimentally expressing catalase, which catalyzes the decomposition of hydrogen peroxide to water and oxygen, in the mitochondria. This has been done using in vitro models (17), adeno-associate viral vectors (AAV) (18), and most recently by genetically engineering its overexpression in mice (19). These transgenic mice, MCat mice, in which the human catalase is targeted to and overexpressed in mitochondria, display a 10–20% increase in maximum and median lifespan (19), reduced age-related insulin resistance (20), and attenuated energy imbalance.

Because mitochondrial targeted overexpression of catalase results in reduced mitochondrial ROS (19, 20), we used the MCat mouse model to investigate the relationship between antioxidant activity and skeletal muscle aging and subsequent functional decline. Aged MCat mice displayed improved voluntary exercise, increased skeletal muscle specific force, increased tetanic Ca^{2+} transients, reduced intracellular Ca^{2+} leak and increased SR Ca^{2+} load compared with age-matched wild-type (WT) littermates. RyR1 channels from aged MCat mice were less oxidized, depleted of calstabin1 and exhibited increased single channel open probability (P_o). Furthermore, pharmacological application of an antioxidant to aged WT RyR1 reduced

Significance

Age-related muscle weakness has major adverse consequences on quality of life, increasing the risk of falls, fractures, and movement impairments. Albeit an increased oxidative state has been shown to contribute to age-dependent reduction in skeletal muscle function, little is known about the mechanisms connecting oxidation and muscle weakness. We show here that genetically enhancing mitochondrial antioxidant activity causes improved skeletal muscle function and voluntary exercise in aged mice. Our findings have broad implications for both the aging and muscle physiology fields, as we present an important molecular mechanism for muscle weakness in aging and skeletal muscle force regulation.

Author contributions: G.S. and A.R.M. designed research; G.S. performed in vivo experiments; A.U., G.S., W.X., and S.R.R. performed ex vivo and in vitro experiments; D.C.A. contributed new reagents/analytic tools; G.S. and A.R.M. analyzed data; and A.U., G.S., and A.R.M. wrote the paper.

Conflict of interest statement: A.R.M. is a consultant for ARMGO, which is targeting RyR channels for therapeutic purposes.

This article is a PNAS Direct Submission.

[1]A.U., G.S., and W.X. contributed equally to this work.

[2]To whom correspondence should be addressed. Email: arm42@columbia.edu.

This article contains supporting information online at www.pnas.org/lookup/suppl/doi:10.1073/pnas.1412754111/-/DCSupplemental.

SR Ca^{2+} leak. We have therefore identified mitochondria as a source of ROS involved in the RyR1 oxidation underlying age-associated skeletal muscle dysfunction.

Results

Six-month-old and 24-mo-old MCat and WT littermates were housed individually for 3 wk in cages equipped with running wheels, and voluntary running performance was recorded. Aged MCat mice exhibited significantly increased running distance relative to age-matched WT mice (Fig. 1*A*). This finding correlated with increased time spent on running wheels (Fig. 1*B*).

To better characterize MCat mice versus WT controls, we performed Masson's trichrome staining on the tibialis anterior muscle. There was no significant difference in the amount of muscle fibrosis when comparing age-matched MCat vs. WT littermates (Fig. S1 *A* and *B*), nor was there a difference in muscle cross-sectional area (Fig. S1*C*). Interestingly, extensor digitorum longus (EDL) muscle weight was lower in aged MCat than in age-matched WT littermates (Fig. S1*D*).

Because MCat mice overexpress human catalase in their mitochondria, mitochondrial integrity was analyzed with electron microscopy. EDL muscle from 24-mo-old WT mice exhibited a significant decrease in cristae density relative to young WT mice (Fig. S2 *A* and *B*). Such a decrease was not observed in aged MCat mice, indicating healthier mitochondria in these mice. Following this trend, mitochondrial ATP synthesis was significantly increased in skeletal muscle mitochondria from aged MCat mice relative to age-matched WT littermates (Fig. S2*C*). Furthermore, aged MCat flexor digitorum brevis (FDB) muscle fibers exhibited reduced mitochondrial ROS levels compared with aged WT (Fig. S2*D*).

To ensure that genetically enhancing mitochondrial catalase reduced oxidative stress on proteins in skeletal muscle we measured advanced oxidation protein products (AOPP). AOPP are uremic toxins created during oxidative stress through the reaction of chlorinated oxidants, including chloramines and hypochlorous acid, with proteins (21). The AOPP content of aged MCat mice was significantly lower than that of WT littermates (Fig. S2*E*). Consistent with these data, the oxidative stress in skeletal muscle nuclear and mitochondrial DNA has been previously reported to be significantly lower in aged (26–29 mo) MCat mice relative to aged WT mice (19). Similarly, the incidence of mitochondrial DNA deletions associated with oxidative damage is lower in aged (18–22 mo old and 33 mo old) MCat mice relative to age-matched WT littermates (19).

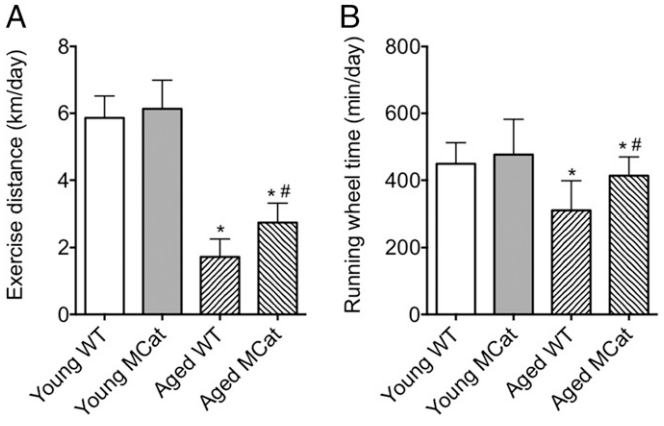

Fig. 1. Improved exercise capacity in aged MCat mice. Mice were housed in individual cages equipped with running wheels for three weeks. Exercise distance (*A*) and running wheel time (*B*) were recorded. Data are mean ± SEM (*$P < 0.01$ vs. young WT; #$P < 0.05$ vs. aged WT; *n*: young WT = 7, young MCat = 8, aged WT = 8, aged MCat = 8, ANOVA).

Because muscle force production is an essential determinant of exercise capacity (22), we hypothesized that this parameter would be affected by the decreased oxidative stress conferred by mitochondrial overexpression of catalase. To test the hypothesis that mitochondrial ROS contribute to age-dependent reduction in skeletal muscle force generating capacity we measured force in EDL muscles from young and aged WT and MCat mice. Isolated EDL muscles were electrically stimulated to contract and force production was measured and normalized to cross-sectional area (yielding a measure of muscle specific force; Fig. 2 *A–D*). There were no significant difference in specific force between young WT and MCat muscles. However, EDL muscle from aged MCat mice exhibited significantly higher specific force than muscles from WT littermates (Fig. 2 *A–D*).

An additional marked feature of skeletal muscle that may account for changes in exercise capacity is its susceptibility to fatigue. Measurement of EDL muscle fatigability was thus accomplished by repeatedly stimulating isolated EDL muscles to tetanic contraction and recording force. The degree of force reduction during fatigue was not different between aged WT and MCat muscles (Fig. S3 *A* and *B*). Furthermore, skeletal muscle twitch contraction was not different among these groups (Fig. S3*C*).

Appropriate SR Ca^{2+} release is essential to skeletal muscle contraction, and we thus studied tetanic Ca^{2+} transients in enzymatically dissociated FDB muscle fibers loaded with the fluorescent Ca^{2+} indicator, Fluo-4 AM. Cells were electrically stimulated to produce tetanic contractions and fluorescence was recorded. Ca^{2+} transients in aged WT and MCat myocytes were markedly reduced relative to young cells. However, this age-dependent reduction in Ca^{2+} transients was significantly improved in aged MCat myocytes (Fig. 3 *A–E*). These changes in Ca^{2+} transients were found in the absence of a significant difference in resting Ca^{2+}. Ca^{2+} content was measured ratiometrically in cells simultaneously loaded with Fluo-4 and Fura-Red and paced to tetanic stimulation (Fig. S4*A*). These results are consistent with our in vivo and ex vivo observations on exercise performance and improved muscle function in aged MCat mice (Figs. 1 and 2).

A major event in skeletal muscle excitation-contraction coupling is Ca^{2+} reuptake by the SR Ca^{2+} ATPase 1 (SERCA1). SERCA1 pumps Ca^{2+} back into the SR following intracellular Ca^{2+} release, lowering the cytosolic [Ca^{2+}] to baseline levels of ∼100 nM, thereby causing relaxation. SERCA1 is tightly regulated by its redox state, and its activity is reduced in aged murine skeletal muscle (23). Thus, we hypothesized that enhanced SERCA activity mechanistically underlies the enhancement of skeletal muscle function in aged MCat muscle. However, activity of SERCA1 in aged WT skeletal muscle was not significantly different from that in aged MCat littermates (Fig. S5*A*). Furthermore, there was no significant difference in SERCA1 tyrosine nitration in MCat vs. age-matched WT littermates (Fig. S5 *B* and *C*). Overall SERCA1 expression in WT vs. MCat littermates was consistent throughout (Fig. S5 *D* and *E*).

We and others have shown that SR Ca^{2+} leak is associated with impaired exercise capacity, defective Ca^{2+} handling, and dysfunctional skeletal muscle performance (15, 24). To test the hypothesis that RyR1-mediated SR Ca^{2+} leak is decreased in aged MCat mice, we measured Ca^{2+} sparks in permeabilized FDB muscles (25). We found a significant reduction in Ca^{2+} spark frequency in aged MCat muscles compared with WT littermates (Fig. 4 *A* and *B*). Additionally, SR Ca^{2+} leak was measured in skeletal muscle microsomes preloaded with Fluo-3. Energized Ca^{2+} load was initiated by adding 0.5 mM ATP and the time course of Ca^{2+} uptake was detected spectrophotometrically. After the Ca^{2+} uptake had reached a plateau, 1 mM thapsigargin was added to inhibit SERCA activity, and the resultant Ca^{2+} leak was monitored. We detected reduced SR Ca^{2+} leak using this alternate method of detection in SR vesicles

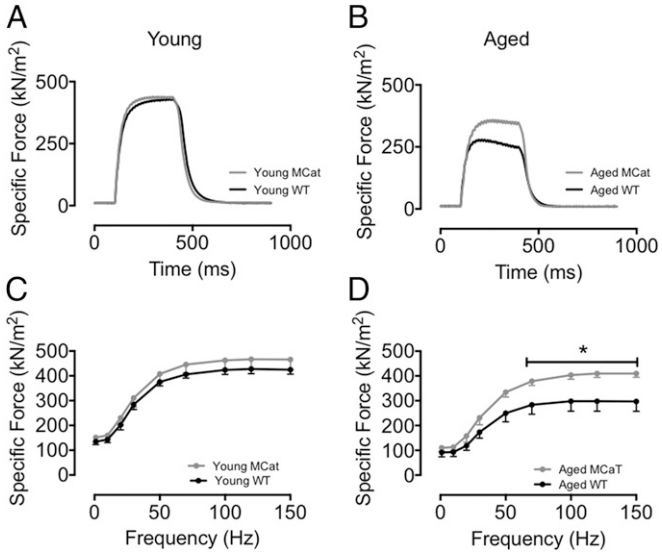

Fig. 2. Preserved skeletal muscle function in aged MCat mice. (*A* and *B*) Tetanic contractions (70 Hz) in isolated EDL muscles from MCat and WT littermates (force normalized to cross-sectional area). (*C* and *D*) Average specific force in EDL muscles from the same mice as in *A* and *B*. Data are mean ± SEM (*n*: young WT = 4, young MCat = 4, aged WT = 8; aged MCat = 7; *t* test was performed for each individual point: $^{*}P < 0.05$ vs. aged WT).

isolated from aged MCat muscles relative to aged WT littermates (Fig. 4 *C* and *D*). Application of the RYR-specific drug, ryanodine, demonstrated RyR1 specificity (Fig. S4*B*).

Depletion of the SR Ca^{2+} store is a consequence of increased SR Ca^{2+} leak in aged skeletal muscle (26). Therefore, we hypothesized that reducing oxidative stress by genetically enhancing mitochondrial catalase activity would prevent this Ca^{2+} depletion in MCat mice. Although SR Ca^{2+} load was reduced in aged WT and MCat relative to their young counterparts, aged MCat muscle exhibited significantly higher SR Ca^{2+} load than aged WT (Fig. 4*E*). Thus, it is likely that the reduced SR Ca^{2+} leak measured in aged MCat mice (Fig. 4 *A*–*D*) results in increased SR Ca^{2+} load, which enhances tetanic Ca^{2+} (Fig. 3 *A*–*D*) and skeletal muscle force production (Fig. 2 *A*–*D*).

Preserved RyR1-calstabin1 interaction is linked to reduced SR Ca^{2+} leak (10, 14). Furthermore, RyR1 oxidation and cysteine nitrosylation decrease the binding affinity of calstabin1 for RyR1 (27, 28), eventually resulting in leaky channels associated with intracellular Ca^{2+} leak and increased Ca^{2+} sparks. Oxidation-dependent posttranslational modifications of RyR1 affect skeletal muscle force generating capacity and this is a key mechanism in age-dependent muscle weakness (10). We therefore examined whether age-dependent oxidative remodeling of the RyR1 macromolecular complex is reduced in MCat mice. RyR1 from aged and young EDL muscles were immunoprecipitated and immunoblotted for components of the RyR1 complex and concomitant redox modifications (10, 14). Age-dependent RyR1 oxidation and cysteine-nitrosylation were both reduced in MCat skeletal muscle, and there was more calstabin1 associated with channels from aged mutant animals compared with WT littermates (Fig. 5 *A* and *B*). Overall expression of neither RyR1 nor calstabin1 was altered in aged WT relative to aged MCat muscles (Fig. S5 *D* and *E*). The relative free thiol content was measured using the specific free thiol-labeling agent, monobromobimane (mBB), in the presence of the pharmacological antioxidant DTT (29). The free thiol content of aged MCat muscle was significantly higher than that of aged WT littermates, indicating reduced RyR1 Cys-oxidation in the aged MCat muscle (Fig. S6 *A* and *B*).

Of interest, reduced RyR1 cysteine nitrosylation in an increased antioxidative environment such as that found in 2-y-old MCat muscle is consistent with the emerging evidence indicating an interplay between Ca^{2+} and oxidative/nitrosative stress (30). Moreover, it has been reported that reactive nitrogen species can substantially modulate catalase and other antioxidant enzymes in skeletal muscle (8, 31, 32). Thus, catalase overexpression may down-regulate cellular levels of nitroxide free radicals, thereby impacting cysteine nitrosylation of RyR1.

The relative effects of calstabin1 depletion, nitrosylation and oxidation on RyR1 activity were dissected with a ligand-binding assay using the RyR1-specific probe, ryanodine, as has been previously published (33). Preferential binding to open RyR1 provides an indirect measure of RyR1 activity (34). Treatment of skeletal SR microsomes with NOC12, a nitric oxide (NO) donor, rapamycin, and the oxidant H_2O_2 increased [^{3}H]ryanodine binding, an indication that oxidation, nitrosylation and calstabin1 depletion from RyR1 each independently cause increased RyR1 activity. Incubation of nitrosylated and/or oxidized samples (35) with calstabin1 +/− the RyR stabilizing rycal drug, S107, significantly reduced RyR1 activity (Fig. S7 *A*–*C*).

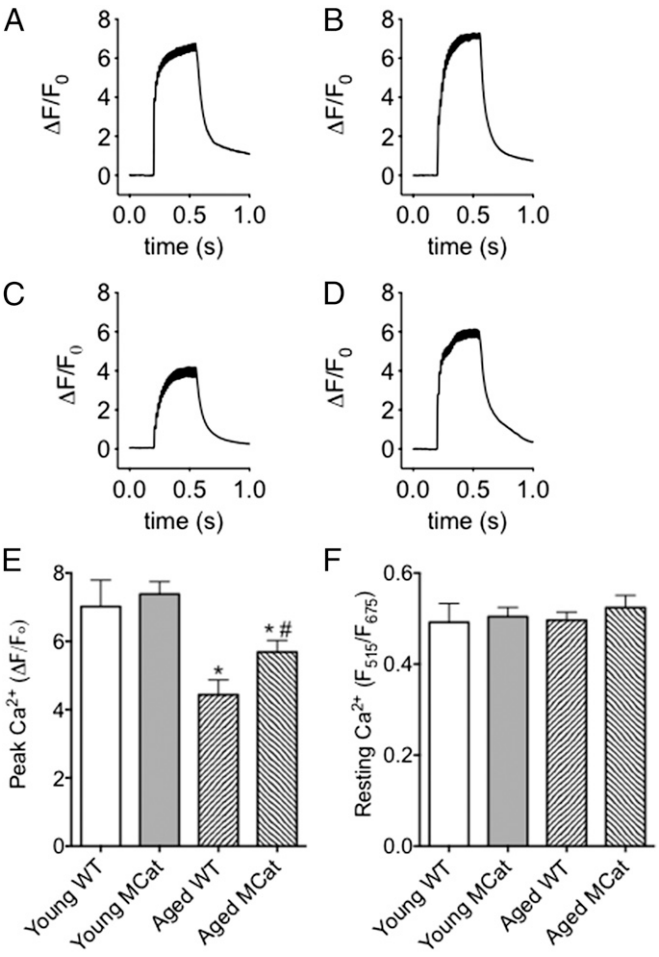

Fig. 3. Improved tetanic Ca^{2+} in skeletal muscle from aged MCat mice. (*A*–*D*) Representative traces of normalized Fluo-4 fluorescence in FDB muscle fibers during a 70 Hz tetanic stimulation in young WT (*A*), young MCat (*B*), aged WT (*C*), and aged MCat (*D*). (*E*) Peak Ca^{2+} responses in FDB fibers stimulated at 70 Hz (fibers taken from the same animals as in *A*–*D*, *n* = 15–21 cells from at least three mice in each group). (*F*) Resting cytosolic Ca^{2+} (measured ratiometrically). Data are mean ± SEM ($^{*}P < 0.05$ vs. young WT; $^{\#}P < 0.05$ vs. aged WT, ANOVA).

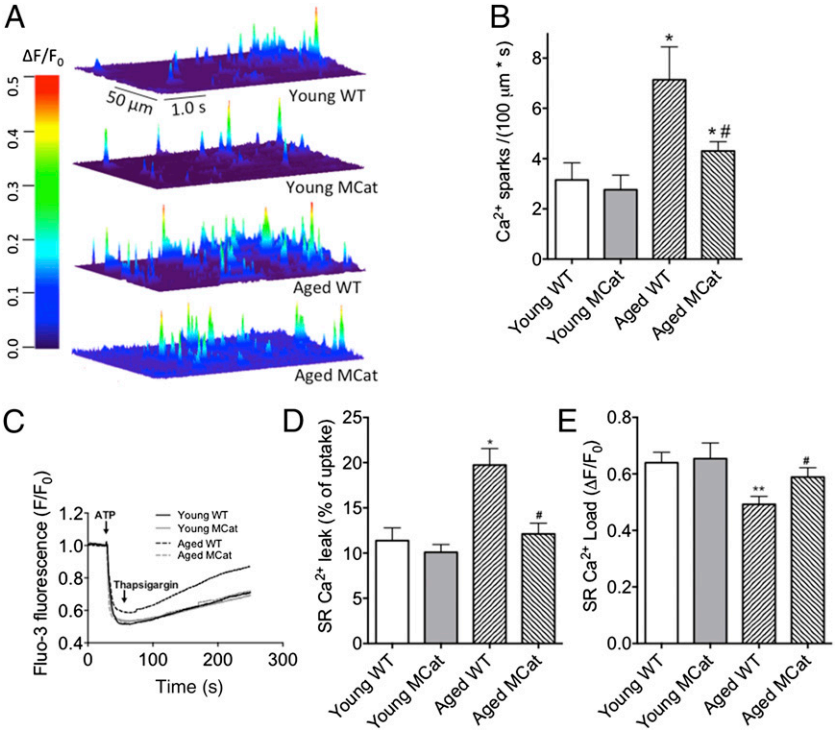

Fig. 4. Reduced SR Ca^{2+} leak and increased SR Ca^{2+} load in muscle from aged MCat mice. (*A*) Representative images of line scans of Fluo-4 fluorescence from permeabilized FDB muscle fibers showing Ca^{2+} spark activity. The heat diagram indicates the normalized change in fluorescence intensity ($\Delta F/F_0$). (*B*) Bar graph showing average Ca^{2+} spark frequency (n = 15–25 cells from at least three mice in each group). (*C*) Representative time course of Ca^{2+} leak from SR microsomes following Ca^{2+} uptake. (*D*) Ca^{2+} leak as calculated by the percentage of uptake. (*E*) SR Ca^{2+} load (measured by applying 1 mM 4-CmC). Data are mean ± SEM (*P < 0.05, **P < 0.01 vs. young WT; $^{\#}P$ < 0.05 vs. aged WT, ANOVA).

To assess the single channel properties of RyR1 in its remodeled state, SR membranes were prepared from EDL muscles and fused to planar lipid membrane bilayers, and Ca^{2+} fluxes through RyR1 channels were recorded (10, 36). The open probability (P_o) of skeletal muscle RyR1 channels from young mice was low, as expected for normal skeletal muscle RyR1 channels (Fig. 5 *C* and *D*). In contrast, skeletal muscle RyR1 channels from aged WT mice exhibited a significantly increased P_o relative to those from aged MCat mice (Fig. 5 *C* and *D*).

Finally, we used a pharmacological approach to demonstrate the causative role of RyR1 oxidation in the described skeletal muscle phenotype. Application of the antioxidant, DTT, to aged murine skeletal muscle caused a significant reduction in the DNP signal associated with immunoblotted RyR1 (Fig. 6 *A* and *B*). SR Ca^{2+} leak (Fig. 6*C*) and RyR1 Ca^{2+} sparks (Fig. 6*D*) were both reduced in aged WT muscle after application of DTT. Therefore, the aged MCat muscle phenotype is likely a result of the antioxidant activity of mitochondrial catalase overexpression.

To rule out the potential influence of oxygen tension, which has been reported to affect RyR1 function (37), we determined that pretreating microsomes with N_2 gas had no significant effect on SR Ca^{2+} leak in aged skeletal muscle (Fig. 6*C*). These data are supported by a more recent study investigating the effects of pO_2 on the activation of RyR1 by NO (38). Although another group found that RyR1 activity is incrementally increased from low (1%) to ambient (20%) O_2, these experiments were conducted on muscle from young mice. RyR1 from aged muscle are highly oxidized (10) and thus a change from low to ambient O_2 levels should not have a significant effect on the oxidation state of the already oxidized channel. Given the fact that young RyR1 activity can increase upon exposure to ambient O_2 levels, the difference between young and aged RyR1 would further increase in the case of low O_2 exposure (38).

Taken together, our data indicate that reducing oxidative stress by genetically enhancing mitochondrial catalase activity in skeletal muscle improves muscle function in aged mice by reducing the loss of calstabin1 from the channel complexes, thus improving channel function. This enhanced channel function results in improved tetanic Ca^{2+} and skeletal muscle specific force in aged mice.

Discussion

In the present study we use a genetic model with enhanced mitochondrial antioxidant activity (MCat mouse model) to investigate the effects of increased antioxidative capacity on age-dependent loss of skeletal muscle function and Ca^{2+} signaling. Our results indicate that MCat mice exhibit reduced age-dependent loss of muscle function. We thus provide compelling evidence for a direct role of mitochondrial free radicals in promoting the pathological intracellular Ca^{2+} leak that underlies age-dependent loss of skeletal muscle function.

Although it has been determined that ectopic catalase overexpression in mitochondria using AAV-9 confers enhanced treadmill performance (18), as measured by exhaustion-limited running distance, neither the underlying mechanism of this observation, nor the effects on age-dependent changes have been reported. Importantly, although RyR1 oxidation has been causally implicated in the reduction of specific force generating capacity in mammalian skeletal muscle (10), the source of these oxidative changes has not been fully established. In the present study we show that mitochondrial ROS is a functionally consequential source of these age-dependent oxidative changes to RyR1. Indeed, mitochondrial targeted overexpression of catalase improves both whole organism (exercise capacity), and skeletal muscle (specific force) performance, and prevents age-dependent reduction in Ca^{2+} transients, reduces age-related biochemical modifications of the SR

Ca^{2+} release channel, and decreases SR Ca^{2+} leak. Furthermore, application of a pharmacological antioxidant to aged skeletal muscle reduces age-dependent SR Ca^{2+} leak.

A growing body of evidence indicates that RyR is tightly regulated by posttranslational modifications involving remodeling of the RyR macromolecular complex (27, 28, 39, 40). Our laboratory has previously shown that RyR1 channels are oxidized, cysteine-nitrosylated and depleted of calstabin1 in muscular dystrophy (14) and in senescence (10), and that these modifications have functional consequences on the Ca^{2+} release channel (15). Intriguingly, here we show that not only age-dependent RyR1 oxidation, but also cysteine nitrosylation is reduced in MCat mice. This finding is consistent with reports that uncovered the capacity of reactive nitrogen species to regulate catalase activity in skeletal muscle (31, 32). Thus, catalase overexpression may down-regulate cellular levels of nitroxide free radicals, thereby impacting cysteine nitrosylation of RyR1. The redox-specific posttranslational modifications that were attenuated in aged MCat mice were consistent with reduced RyR1-mediated SR Ca^{2+} leak. This is in agreement with studies in which prolonged exposure to NO donors has been shown to increase the SR Ca^{2+} leak and resting cytosolic Ca^{2+} in voltage-clamped mouse FDB fibers (41). Additionally, inhibiting RyR1-mediated SR Ca^{2+} leak results in rescue of age-dependent increase in spontaneous releases of SR Ca^{2+} (Ca^{2+} sparks) in permeabilized FDB muscle fibers, as shown in aged MCat muscle fibers in the present study.

We conclude that mitochondrial ROS have a causative role in mediating age-dependent redox modifications of RyR1 and consequently play a key role in the regulation of age-dependent loss of skeletal muscle function. Not only do our results have substantial translational implications for the development of novel therapeutic strategies, such as mitochondria-targeted antioxidants for treatment of mitochondrial myopathies, ROS mediated muscular dysfunctions and other healthspan limiting disorders (12, 42), we also present a molecular mechanism for age-dependent skeletal muscle weakness and regulation of musculoskeletal force generation.

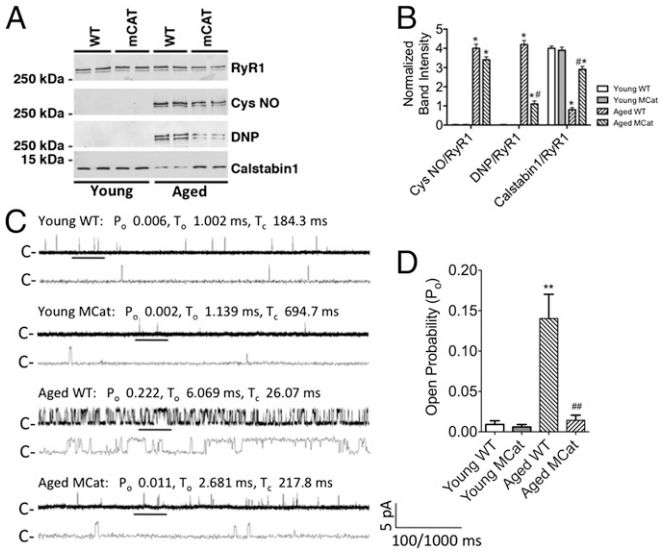

Fig. 5. Skeletal muscle RyR1 isolated from aged MCat mice is remodeled and exhibits reduced single-channel open probability (P_o). (*A*) Representative immunoblots from triplicate experiments of immunoprecipitated RyR1 from aged murine EDL. (*B*) Bar graphs showing quantification of the immunoblots in *A*; DNP: 2,4-dinitrophenylhydrazone. (*C*) Representative RyR1 single-channel current traces. Channel openings are shown as upward deflections and the closed (c-) state of the channel is indicated by horizontal bars in the beginning of each trace. Tracings from over 2 min of recording for each condition showing channel activity at two time scales (5 s in upper trace and 500 ms in lower trace) as indicated by dimension bars, and the respective P_o (open probability), T_o (average open time), and T_c (average closed time) are shown above each trace. The activity of the channel indicated by the thick black bar is shown on the expanded time scale (the 500 ms trace below). (*D*) Bar graph summarizing P_o at 150 nM cytosolic [Ca^{2+}] in young WT ($n = 6$), aged WT ($n = 5$), young MCat ($n = 7$), and aged MCat ($n = 5$) channels. Data are mean ± SEM (*$P < 0.05$, **$P < 0.01$ vs. young WT, #$P < 0.05$, ##$P < 0.01$ vs. aged WT, ANOVA).

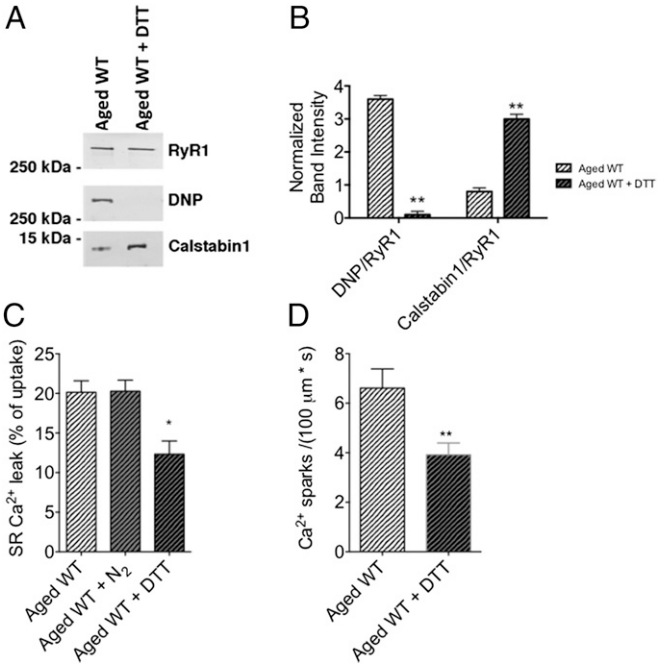

Fig. 6. Antioxidant application to aged WT skeletal muscle reduces age-associated SR Ca^{2+} leak. (*A*) Representative immunoblot of immunoprecipitated RyR1 from aged murine skeletal muscle. For DTT treatment, SR vesicles were preincubated with 1 mM DTT. (*B*) Bar graphs showing quantification of the immunoblots in *A*. (*C*) Bar graph representing Ca^{2+} leak in SR microsomes of skeletal muscles from aged WT mice. For N_2 treatment, solutions was prebubbled with 100% N_2 for 1 h. (*D*) Bar graph representing average Ca^{2+} spark frequency in permeabilized FDB muscle fibers from aged WT mice. Data are mean ± SEM (n = 19–22 cells from three mice per group; *$P < 0.05$ vs. aged WT; **$P < 0.01$ vs. aged WT, ANOVA).

Materials and Methods

See *SI Materials and Methods* for additional and detailed descriptions.

Ethical Approval. The use and maintenance of mice was in accordance with Columbia University Institutional Animal Care and Use Committee regulations and with the Guide for the Care and Use of Laboratory Animals published by the National Institutes of Health (43).

Statistics. In all of the experiments mice were coded to 'blind' investigators with respect to genotype. The sample size (n in each group) for each experiment is stated in the figure legends. Data are expressed as mean ± SE (SEM), unless otherwise indicated. To determine statistical significance, we used two-way ANOVA and comparison t test, as appropriate. Bonferroni post hoc testing was performed where applicable. Minimum statistically significant differences were established at $P < 0.05$.

ACKNOWLEDGMENTS. We thank Peter S. Rabinovitch (University of Washington) for generously providing the MCat mouse founders. We also thank Bi-Xing Chen (Columbia University) for technical support. This study was supported by American Heart Association Grants AHA13POST16810041 (to G.S.) and AHA11PRE7810019 (to A.U.), by the Swedish Heart Lung Foundation (to D.C.A.), and by grants from the National Heart, Lung, and Blood Institute and from the Ellison Foundation (to A.R.M.).

1. Clegg A, Young J, Iliffe S, Rikkert MO, Rockwood K (2013) Frailty in elderly people. *Lancet* 381(9868):752–762.
2. Boockvar KS, Meier DE (2006) Palliative care for frail older adults: "There are things I can't do anymore that I wish I could . . .". *JAMA* 296(18):2245–2253.
3. Short KR, et al. (2005) Decline in skeletal muscle mitochondrial function with aging in humans. *Proc Natl Acad Sci USA* 102(15):5618–5623.
4. Roubenoff R, Castaneda C (2001) Sarcopenia-understanding the dynamics of aging muscle. *JAMA* 286(10):1230–1231.
5. Sardu C, Marfella R, Santulli G (2014) Impact of diabetes mellitus on the clinical response to cardiac resynchronization therapy in elderly people. *J Cardiovasc Transl Res* 7(3):362–368.
6. Harman D (1956) Aging: A theory based on free radical and radiation chemistry. *J Gerontol* 11(3):298–300.
7. Balaban RS, Nemoto S, Finkel T (2005) Mitochondria, oxidants, and aging. *Cell* 120(4): 483–495.
8. Santulli G, Iaccarino G (2013) Pinpointing beta adrenergic receptor in ageing pathophysiology: Victim or executioner? Evidence from crime scenes. *Immun Ageing* 10(1):10.
9. Martin GM, Loeb LA (2004) Ageing: Mice and mitochondria. *Nature* 429(6990): 357–359.
10. Andersson DC, et al. (2011) Ryanodine receptor oxidation causes intracellular calcium leak and muscle weakness in aging. *Cell Metab* 14(2):196–207.
11. Finley LW, et al. (2012) Skeletal muscle transcriptional coactivator PGC-1α mediates mitochondrial, but not metabolic, changes during calorie restriction. *Proc Natl Acad Sci USA* 109(8):2931–2936.
12. Santulli G, Ciccarelli M, Trimarco B, Iaccarino G (2013) Physical activity ameliorates cardiovascular health in elderly subjects: The functional role of the β adrenergic system. *Front Physiol* 4:209.
13. Allen DG, Lamb GD, Westerblad H (2008) Skeletal muscle fatigue: Cellular mechanisms. *Physiol Rev* 88(1):287–332.
14. Bellinger AM, et al. (2009) Hypernitrosylated ryanodine receptor calcium release channels are leaky in dystrophic muscle. *Nat Med* 15(3):325–330.
15. Bellinger AM, et al. (2008) Remodeling of ryanodine receptor complex causes "leaky" channels: A molecular mechanism for decreased exercise capacity. *Proc Natl Acad Sci USA* 105(6):2198–2202.
16. Ahern GP, Junankar PR, Dulhunty AF (1997) Subconductance states in single-channel activity of skeletal muscle ryanodine receptors after removal of FKBP12. *Biophys J* 72(1):146–162.
17. Bai J, Rodriguez AM, Melendez JA, Cederbaum AI (1999) Overexpression of catalase in cytosolic or mitochondrial compartment protects HepG2 cells against oxidative injury. *J Biol Chem* 274(37):26217–26224.
18. Li D, et al. (2009) Ectopic catalase expression in mitochondria by adeno-associated virus enhances exercise performance in mice. *PLoS ONE* 4(8):e6673.
19. Schriner SE, et al. (2005) Extension of murine life span by overexpression of catalase targeted to mitochondria. *Science* 308(5730):1909–1911.
20. Lee HY, et al. (2010) Targeted expression of catalase to mitochondria prevents age-associated reductions in mitochondrial function and insulin resistance. *Cell Metab* 12(6):668–674.
21. Anderson DR, et al. (2010) Albumin-based microbubbles bind up-regulated scavenger receptors following vascular injury. *J Biol Chem* 285(52):40645–40653.
22. Rantanen T, et al. (1999) Midlife hand grip strength as a predictor of old age disability. *JAMA* 281(6):558–560.
23. Viner RI, Williams TD, Schöneich C (1999) Peroxynitrite modification of protein thiols: Oxidation, nitrosylation, and S-glutathiolation of functionally important cysteine residue(s) in the sarcoplasmic reticulum Ca-ATPase. *Biochemistry* 38(38):12408–12415.
24. Wang X, et al. (2005) Uncontrolled calcium sparks act as a dystrophic signal for mammalian skeletal muscle. *Nat Cell Biol* 7(5):525–530.
25. Isaeva EV, Shkryl VM, Shirokova N (2005) Mitochondrial redox state and Ca2+ sparks in permeabilized mammalian skeletal muscle. *J Physiol* 565(Pt 3):855–872.
26. Romero-Suarez S, et al. (2010) Muscle-specific inositide phosphatase (MIP/MTMR14) is reduced with age and its loss accelerates skeletal muscle aging process by altering calcium homeostasis. *Aging (Albany, NY Online)* 2(8):504–513.
27. Aracena-Parks P, et al. (2006) Identification of cysteines involved in S-nitrosylation, S-glutathionylation, and oxidation to disulfides in ryanodine receptor type 1. *J Biol Chem* 281(52):40354–40368.
28. Eu JP, Xu L, Stamler JS, Meissner G (1999) Regulation of ryanodine receptors by reactive nitrogen species. *Biochem Pharmacol* 57(10):1079–1084.
29. Sun J, Xu L, Eu JP, Stamler JS, Meissner G (2001) Classes of thiols that influence the activity of the skeletal muscle calcium release channel. *J Biol Chem* 276(19): 15625–15630.
30. Hidalgo C, Donoso P (2008) Crosstalk between calcium and redox signaling: From molecular mechanisms to health implications. *Antioxid Redox Signal* 10(7):1275–1312.
31. Trebak M, Ginnan R, Singer HA, Jourd'heuil D (2010) Interplay between calcium and reactive oxygen/nitrogen species: An essential paradigm for vascular smooth muscle signaling. *Antioxid Redox Signal* 12(5):657–674.
32. Lawler JM, Song W (2002) Specificity of antioxidant enzyme inhibition in skeletal muscle to reactive nitrogen species donors. *Biochem Biophys Res Commun* 294(5): 1093–1100.
33. Meissner G, Rios E, Tripathy A, Pasek DA (1997) Regulation of skeletal muscle Ca2+ release channel (ryanodine receptor) by Ca2+ and monovalent cations and anions. *J Biol Chem* 272(3):1628–1638.
34. Sutko JL, Airey JA, Welch W, Ruest L (1997) The pharmacology of ryanodine and related compounds. *Pharmacol Rev* 49(1):53–98.
35. Mei Y, et al. (2013) Stabilization of the skeletal muscle ryanodine receptor ion channel-FKBP12 complex by the 1,4-benzothiazepine derivative S107. *PLoS ONE* 8(1): e54208.
36. Brillantes AB, et al. (1994) Stabilization of calcium release channel (ryanodine receptor) function by FK506-binding protein. *Cell* 77(4):513–523.
37. Eu JP, Sun J, Xu L, Stamler JS, Meissner G (2000) The skeletal muscle calcium release channel: Coupled O2 sensor and NO signaling functions. *Cell* 102(4):499–509.
38. Cheong E, Tumbev V, Stoyanovsky D, Salama G (2005) Effects of pO2 on the activation of skeletal muscle ryanodine receptors by NO: A cautionary note. *Cell Calcium* 38(5): 481–488.
39. Xia R, Stangler T, Abramson JJ (2000) Skeletal muscle ryanodine receptor is a redox sensor with a well defined redox potential that is sensitive to channel modulators. *J Biol Chem* 275(47):36556–36561.
40. Durham WJ, et al. (2008) RyR1 S-nitrosylation underlies environmental heat stroke and sudden death in Y522S RyR1 knockin mice. *Cell* 133(1):53–65.
41. Pouvreau S, Allard B, Berthier C, Jacquemond V (2004) Control of intracellular calcium in the presence of nitric oxide donors in isolated skeletal muscle fibres from mouse. *J Physiol* 560(Pt 3):779–794.
42. Schapira AH (2012) Mitochondrial diseases. *Lancet* 379(9828):1825–1834.
43. National Research Council Institute for Laboratory Animal Research (1996) *Guide for the Care and Use of Laboratory Animals* (National Academies, Washington, DC).

Supporting Information

Umanskaya et al. 10.1073/pnas.1412754111

SI Materials and Methods

Animals. MCat mouse model generation has been described (1). MCat founders were kindly provided by Peter S. Rabinovitch (University of Washington, Seattle) and backcrossed >9 generations onto C57BL/6 background. We used 6-mo-old (young) and 24-mo-old (aged) male MCat mice and their age-matched WT littermates. The rodents were housed in a 22 °C room with a 12-h light/dark cycle and were allowed food and water ad libitum. Blinded observers performed all experiments.

Voluntary Exercise. Analysis of voluntary exercise was performed using individual cages equipped with running wheels. To minimize environmental differences, mice were allowed to acclimate to the running wheels for a period of at least 7 d and then exercise on the wheel was continuously recorded for 2 wk using a data acquisition system (Minimitter, Bend, OR). Mice were euthanized and muscles were quickly harvested for functional and biochemical analyses.

Histology. Histological analysis of tibialis anterioris muscles was performed as described and validated (2, 3). Briefly, the samples were fixed in buffered paraformaldehyde and processed for paraffin embedding (4). For Masson's trichrome staining, slides were stained with Weigert Hematoxylin (Sigma-Aldrich) for 10 min, rinsed in PBS and then stained with Biebrich scarlet-acid fuchsin (Sigma-Aldrich) for 5 min (5). Slides were then washed and stained with phosphomolybdic/phosphotungstic acid solution (Sigma-Aldrich) and with light green (Sigma-Aldrich), as described (6). Percent collagen was calculated from high-resolution, color-calibrated digital images of Masson's trichrome–stained sections with the use of dedicated software (FIJI). Cross-sectional area was measured as described (3, 5).

Transmission Electron Microscopy. EDL muscles were fixed in 2.5% glutaraldehyde in 0.1M Sørensen's buffer and postfixed in 1% OsO_4 (7). Following dehydration, samples were embedded in Lx-112 (Ladd Research Industries). After cutting (ultramicrotome MT-7000), 60 nm sections were stained with uranyl acetate and lead citrate and visualized (JEM-1400, JEOL) at the Electron Microscopy and Histology and Optical Microscopy Core Facilities of Weill Cornell Medical College, New York. At least eight sections for each group were used for the analysis of mitochondrial morphology. To quantify the cristae density a computerized point grid was digitally layered over the micrographic images, as described (8, 9). The investigators were blinded to the genotype, age and treatment of the groups.

Mitochondrial Bioenergetics. ATP synthesis rates in skeletal muscle were determined using a bioluminescence kit (Sigma-Aldrich), as described (7). Briefly, 10 μg of skeletal muscle (tibialis anterior) mitochondria were dissolved in 50 μL of buffer (10 mM Hepes, 125 mM KCl, 5 mM $MgCl_2$, 2 mM K_2HPO_4, pH 7.42) to determine complex I (5 mM pyruvate/malate) or complex II (5 mM succinate) driven ATP synthesis. To determine the rates of non-mitochondrial ATP production, measurements with substrates were repeated in presence (0.5 μM) of inhibitors of respiratory complex: rotenone (complex I), antimycin (complex III), and oligomycin (complex IV). To avoid the reverse electron transfer effect, succinate-driven ATP synthesis was assessed in the presence of rotenone (0.5 μM).

Mitochondrial Superoxide Detection. FDB fibers were incubated for 20 min at room temperature with MitoSOX Red (Thermo Fisher Scientific; 2.5 μM), a mitochondria-targeted fluorescent indicator for ROS. Cells were stimulated with H_2O_2 (100 μM), as described (10), whereas Antimycin A (10 μM) was added at the end of the experiment to induce an increase in mitochondrial superoxide production. Using a confocal microscope (Zeiss LSM 5 Live, 40× oil immersion lens), MitoSOX-loaded cells were excited at 488 nm and the emitted signal was filtered through a band pass filter (540–625 nm).

Advanced Oxidation Protein Products (AOPP) Measurement. AOPP in muscle tissue lysates were determined using the AOPP Assay Kit from Cell Biolabs as per manufacturer's instructions. Briefly, tissue homogenate (0.5 mg) was diluted to a total of 0.2 mL in PBS and added to three wells of a microtiter plate. The chloramine reaction initiator (10 μL) was added to each well. Samples were mixed thoroughly by pipetting and incubated at room temperature for 5 min. Reactions were stopped with 20 μL of stop solution added to each well. The reactions were mixed thoroughly. The absorbance at 340 nM of each well was determined using a spectrophotometric plate reader. The AOPP content was determined by comparison with the predetermined Chloramine standard curve.

Muscle Function. The specific force of whole extensor digitorum longus (EDL) muscles was assessed ex vivo using a system from Aurora Scientific. EDL muscles were dissected and stainless steel hooks were tied to the tendons of the muscles using nylon sutures and the muscles were mounted between a force transducer (Harvard Apparatus, Holliston, MA) and an adjustable hook. The muscles were immersed in a stimulation chamber containing O_2/CO_2 (95/5%) bubbled Tyrode solution (121 mM NaCl, 5.0 mM KCl, 1.8 mM $CaCl_2$, 0.5 mM $MgCl_2$, 0.4 mM NaH_2PO_4, 24 mM $NaHCO_3$, 0.1 mM EDTA, 5.5 mM glucose). The muscle was stimulated to contract using an electrical field between two platinum electrodes. At the start of each experiment the muscle length was adjusted to yield the maximum force. The force–frequency relationships were determined by triggering contraction using incremental stimulation frequencies (EDL: 0.5-ms pulses at 2–150 Hz for 350 ms at suprathreshold voltage). Between stimulations the muscle was allowed to rest for ∼1 min. The fatigue protocol consisted of 50 tetanic contractions (70 Hz, 350 ms duration) given at 2-s intervals. At the end of the force measurement, the length and weight of the muscle was measured and the muscle was snap frozen in liquid nitrogen. To quantify the specific force, the absolute force was normalized to the muscle cross-sectional area, calculated as the muscle weight divided by the length using a muscle density constant of 1.056 kg × m^{-3}.

Ca^{2+} Transients Measurement. Single flexor digitorum brevis (FDB) fibers were obtained by enzymatic dissociation. FDB muscles from both hind limbs were incubated for ∼2 h at 37 °C in ∼4 mL Dulbecco's Modified Eagles Medium (DMEM) containing 0.3% collagenase 1 (Sigma) and 10% FBS. The muscles were transferred to a culture dish containing fresh DMEM (∼4 mL) and gently triturated until the muscles were dissociated. The cell suspension was stored in an incubator at 37 °C/5% CO_2 until the start of the experiment.

FDB fibers were loaded with the fluorescent Ca^{2+} indicator fluo-4 acetoxymethyl ester (AM; 5 μM, Invitrogen/Molecular Probes) for 15 min at room temperature. The cells were allowed

to attach to a laminin-coated glass coverslip that formed the bottom of a perfusion chamber. The cells were then superfused with Tyrode solution [121 mM NaCl, 5.0 mM KCl, 1.8 mM $CaCl_2$, 0.5 mM $MgCl_2$, 0.4 mM NaH_2PO_4, 24 mM $NaHCO_3$, 0.1 mM EDTA, 5.5 mM glucose; bubbled with O_2/CO_2 (95/5%)]. The fibers were triggered to twitch contraction using electrical field stimulation (pulses of 0.5 ms at suprathreshold voltage) and fluo-4 fluorescence was monitored using a confocal microscope system (Zeiss LSM 5 Live, 40× oil immersion lens, excitation wavelength was 488 nm and the emitted fluorescence was recorded between 495 and 525 nm). The use of single excitation/emission dye Fluo-4 necessitates normalizing to prestimulation values to negate possible differences in dye loading and excitation strength. Only fibers attached to the bottom of the perfusion chamber throughout the twitch stimulation were measured from.

SERCA1 Activity Assay. SERCA activity was measured using the malachite green procedure for phosphate determination, adapted to the microscale as described (11). The reaction was started by the addition of 50 μg of muscle microsomes to 150 μl of reaction mixture (20 mM Mops/Tris·HCl, pH 6.8. 100 mM KCl, 5 mM $MgCl_2$, 5 mM ATP, 1 mM EGTA. 0.350 mM $CaCl_2$ (free Ca^{2+} concentration of ∼500 nM as calculated using the CHELATOR program). After 5 min, the reaction was stopped by the transfer of 120 μl of reaction mixture to 80 μl of malachite green reagent mixture in a 96-well microplate. The malachite green reagent mixture was made by mixing 0.122% malachite green hydrochloride in 6.2 N H_2SO_4, 5.76% ammonium paramolybdate tetrahydrate, and 11% Tween 20 in a volume ratio of 100:66:2. Color development was quenched after 10 s by the addition of 45 μl of 15.1% sodium citrate dihydrate. Inorganic phosphate liberated in the ATPase reaction was quantified by comparison of absorbance at 570 nm with standard curves generated with known amounts of Na_2HPO_4 in the reaction buffer.

Ca^{2+} Sparks Measurement. For Ca^{2+} sparks measurements, FDB muscle fibers were permeabilized in a relaxing solution (140 mM K-glutamate, 10 mM Hepes, 10 mM MgCl2, 0.1 mM EGTA, pH 7.0) containing 0.01% saponin for ∼1 min. After washing the sample with a saponin free solution, the solution was changed to an internal medium [140 mM potassium L-glutamate, 5 mM Na2ATP, 10 mM glucose, 10 mM Hepes, 4.4 mM MgCl2, 1.1 mM EGTA, 0.3 mM CaCl2 (free [Ca^{2+}] 130 nM), Fluo-3 0.05; pentapotassium salt, Invitrogen; pH 7.0]. Fluorescence images were acquired with a Zeiss LSM 5 Live confocal system (63× oil immersion, NA = 1.4) operated in line-scan mode (*x* vs. *t*, 2 ms per line, 5,000 lines per scan) along the longitudinal axis of the fibers. Fluo-3 was excited with an Argon laser at 488 nm, and the emitted fluorescence was recorded between 495–555 nm. Ca^{2+} sparks detection and analyses used custom made routines compiled in IDL (v7.1, ITT) according to algorithms described previously (12, 13).

Quantification of RyR1 Thiol Content. The number of free thiols in RyR1 was determined as described (14). Briefly, SR microsomes isolated from mouse hind limb muscle were incubated probed with an excess (20 mM) of the lipophilic, thiol-specific agent, mBB, for 1 h in the dark at room temperature. Following mBB treatment, RyR1 was immunoprecipitated using the RyR-5029 antibody from 50 μg of SR. The RyR1 complex was eluted from the immunoprecipitate using 100-fold excess of 5029 peptide. Each sample was split to determine mBB fluorescence intensity and RyR1 levels (by Western blot analysis). RyR1 oxidation was normalized to maximum RyR1 thiol oxidation obtained with 10 mM DTT treatment of control SR.

[^{3}H]Ryanodine Binding. Rabbit Skeletal SR microsomes were treated for 45 min at room temperature with either 1.0 μM rapamycin, 100 μM NOCl2, 1 mM H_2O_2, or 100 μM NOCl2 followed by 1 mM H_2O_2. Nitrosylated and/or oxidized samples were incubated with 20 nM calstabin1 ± S107 for 1 h at room temperature. SR was incubated with 3 nM [^{3}H]ryanodine at 24 °C in 0.25 M KCl, 20 mM imidazole, pH 7.0 with ∼7 μM free Ca^{2+} and protease inhibitors. Nonspecific binding was determined using 1,000-fold excess of unlabeled ryanodine (15). After 5 h, aliquots of the samples were diluted with 20 volumes of ice-cold water and placed on Whatman filters presoaked with 2% polyethyleneimine (16). Filters were washed and the radioactivity remaining on the filters was determined by liquid scintillation counting (4, 17).

Immunoprecipitation and Immunoblot Analysis. Muscle samples (EDL) were isotonically lysed in 0.5 mL of buffer containing 50 mM Tris·HCl (pH 7.4), 150 mM NaCl, 20 mM NaF, 1.0 mM Na_3VO_4 and protease inhibitors. The samples were incubated with the antibody in 0.5 mL of a modified RIPA buffer (50 mM Tris–HCl pH 7.4, 0.9% NaCl, 5.0 mM NaF, 1.0 mM Na_3VO_4, 1% Triton-X100 and protease inhibitors) for 1 h at 4 °C. The immune complexes were incubated with protein A Sepharose beads (Sigma) at 4 °C for 1 h and the beads were washed three times with buffer. Proteins were separated on SDS/PAGE gels (6% for RyR1, 15% for calstabin1, 10% for SERCA1) and transferred on to nitrocellulose membranes for 2 h at 200 mA (SemiDry transfer blot, Bio-Rad). Immunoblots were developed using the following primary antibodies: anti-RyR1 (1:2,000, Thermo Scientific), anti-phospho-RyR1-pSer2844 (1:5,000), anti-calstabin (FKBP12 C-19, 1:1,000, Santa Cruz Biotechnology), anti-Cys-NO (1:1,000, Sigma-Aldrich), anti-SERCA1 (1:1,000, Abcam), anti-n-tyrosine (1:1,000, Abcam). To determine channel oxidation, the carbonyl groups in the protein side chains within the immunoprecipitate were derivatized to 2,4-dinitrophenylhydrazone (DNP) by reaction with 2,4-dinitrophenylhydrazine. The DNP signal associated with RyR was determined using a specific anti-DNP antibody, according to the manufacturer's instructions (Millipore). Levels of RyR1 bound proteins were normalized to the total RyR1 immunoprecipitated (arbitrary units). All immunoblots were developed with the Odyssey system (LI-COR Biosciences), using IR-labeled anti-mouse and anti-rabbit IgG (1:10000 dilution) secondary antibodies, as described (18).

Single Channel Recordings. Muscles were homogenized using a tissue homogenizer (Fisher Scientific) at the highest speed for 1 min with 2 volumes of 20 mM Tris-maleate (pH 7.4), 1 mM EDTA and protease inhibitors (Roche). Homogenate was centrifuged at 4,000 × *g* for 15 min at 4 °C and the supernatant was centrifuged at 40,000 × *g* for 30 min at 4 °C. The final pellet, containing the SR fractions, was resuspended and aliquoted in: 250 mM sucrose, 10 mM Mops (pH 7.4), 1 mM EDTA and protease inhibitors. Samples were frozen in liquid nitrogen and stored at −80 °C. SR vesicles containing RyR1 were fused to planar lipid bilayers formed by painting a lipid mixture of phosphatidylethanolamine and phosphatidylcholine (Avanti Polar Lipids) in a 3:1 ratio across a 200-μm hole in polysulfonate cups (Warner Instruments) separating two chambers. The trans chamber (1.0 mL), representing the intra-SR (luminal) compartment, was connected to the head stage input of a bilayer voltage clamp amplifier. The *cis* chamber (1.0 mL), representing the cytoplasmic compartment, was held at virtual ground. Symmetrical solutions used were as follows: 1 mM EGTA, 250/125 mM Hepes/Tris, 50 mM KCl, 0.64 mM $CaCl_2$, pH 7.35 as *cis* solution and 53 mM $Ca(OH)_2$, 50 mM KCl, 250 mM Hepes, pH 7.35 as *trans* solution. The concentration of free Ca^{2+} in the *cis* chamber was calculated with WinMaxC program (version 2.50; www.stanford.edu/∼cpatton/maxc.html). SR vesicles were added to the *cis* side and fusion with the lipid bilayer was induced by making the *cis* side hyperosmotic by the addition of 500 mM KCl. After the appearance of potassium and chloride channels,

the *cis* side was perfused with the *cis* solution. Single-channel currents were recorded at 0 mV by using a Bilayer Clamp BC-525C (Warner Instruments), filtered at 1 kHz using a Low-Pass Bessel Filter 8 Pole (Warner Instruments), and digitized at 4 kHz. All experiments were performed at room temperature (23 °C). Data acquisition was performed by using Digidata 1322A and Axoscope 10.1 software (Axon Instruments). The recordings were analyzed by using Clampfit 10.1 (Molecular Devices) and Origin software (ver. 6.0, Microcal Software).

Measurement of Ca^{2+} Leak from SR Vesicles. Murine SR vesicle (0.2 mg) was added in 1-mL solutions including: 150 mM potassium D-gluconate, 1 mM $MgCl_2$, 0.1 mM EGTA-Ca^{2+} buffer (free [Ca^{2+}] 0.3 μM), 10 mM NaN_3, 20 mM Mops, 0.02 mM fluo-3, pH 6.8. Ca^{2+} uptake was initiated by addition of 0.5 mM ATP, and the time course of Ca^{2+} uptake was monitored spectrophotometrically. After the Ca^{2+} uptake had reached a plateau, 1 mM thapsigargin was added to inhibit SERCA activity, and the resultant Ca^{2+} leak was monitored. The Ca^{2+} leak was expressed as the ratio of the amount of Ca^{2+} leaked out from the SR at 60 s after the addition of thapsigargin to the amount of total Ca^{2+} uptake (19).

SR Ca^{2+} Load Determination in Isolated FDB Muscle Cells. FDB muscle cells were preloaded with 5 μM low-affinity Ca^{2+} dye mag-fluo-4 for 30 min, then 1 mM 4-CmC was applied to cells to induce maximum release. Mag-fluo-4 was excited at 488 nm and emission was collected at 495–525.

Resting [Ca^{2+}] Determination. Resting [Ca^{2+}] in FDB muscle cells were ratiometrically measured with fluo-4 and fura-red as described (20). FDB muscle cells were simultaneously loaded with 5 μM fluo-4 AM and 10 μM fura-red for 10 min. They were then excited at 488 nm and emission was collected at 495–525 (F_{515}) and 650–700 (F_{675}), respectively. The ratio of the two emissions represents [Ca^{2+}].

1. Schriner SE, et al. (2005) Extension of murine life span by overexpression of catalase targeted to mitochondria. *Science* 308(5730):1909–1911.
2. Santulli G, et al. (2009) In vivo properties of the proangiogenic peptide QK. *J Transl Med* 7:41.
3. Santulli G, et al. (2012) CaMK4 gene deletion induces hypertension. *J Am Heart Assoc* 1(4):e001081.
4. Santulli G, et al. (2012) Age-related impairment in insulin release: The essential role of β(2)-adrenergic receptor. *Diabetes* 61(3):692–701.
5. Sorriento D, et al. (2010) Intracardiac injection of AdGRK5-NT reduces left ventricular hypertrophy by inhibiting NF-kappaB-dependent hypertrophic gene expression. *Hypertension* 56(4):696–704.
6. Santulli G, et al. (2011) Evaluation of the anti-angiogenic properties of the new selective αVβ3 integrin antagonist RGDechiHCit. *J Transl Med* 9:7.
7. Fusco A, et al. (2012) Mitochondrial localization unveils a novel role for GRK2 in organelle biogenesis. *Cell Signal* 24(2):468–475.
8. Karamanlidis G, et al. (2013) Mitochondrial complex I deficiency increases protein acetylation and accelerates heart failure. *Cell Metab* 18(2):239–250.
9. Phoon CK, et al. (2012) Tafazzin knockdown in mice leads to a developmental cardiomyopathy with early diastolic dysfunction preceding myocardial noncompaction. *J Am Heart Assoc* 1(2):jah3-e000455.
10. Aydin J, et al. (2009) Increased mitochondrial calcium and decreased sarcoplasmic reticulum Ca^{2+} in mitochondrial myopathy. *Hum Mol Genet* 18(2):278–288.
11. Kimura Y, Kurzydlowski K, Tada M, MacLennan DH (1996) Phospholamban regulates the Ca2+-ATPase through intramembrane interactions. *J Biol Chem* 271(36):21726–21731.
12. Xie W, et al. (2013) Imaging atrial arrhythmic intracellular calcium in intact heart. *J Mol Cell Cardiol* 64:120–123.
13. Cheng H, et al. (1999) Amplitude distribution of calcium sparks in confocal images: theory and studies with an automatic detection method. *Biophys J* 76(2):606–617.
14. Sun J, Xu L, Eu JP, Stamler JS, Meissner G (2001) Classes of thiols that influence the activity of the skeletal muscle calcium release channel. *J Biol Chem* 276(19): 15625–15630.
15. Meissner G, Rios E, Tripathy A, Pasek DA (1997) Regulation of skeletal muscle Ca2+ release channel (ryanodine receptor) by Ca2+ and monovalent cations and anions. *J Biol Chem* 272(3):1628–1638.
16. Perino A, et al. (2011) Integrating cardiac PIP3 and cAMP signaling through a PKA anchoring function of p110γ. *Mol Cell* 42(1):84–95.
17. Ciccarelli M, et al. (2008) Endothelial alpha1-adrenoceptors regulate neo-angiogenesis. *Br J Pharmacol* 153(5):936–946.
18. Santulli G, et al. (2014) A selective microRNA-based strategy inhibits restenosis while preserving endothelial function. *J Clin Invest* 124(9):4102–4114.
19. Tateishi H, et al. (2009) Defective domain-domain interactions within the ryanodine receptor as a critical cause of diastolic Ca2+ leak in failing hearts. *Cardiovasc Res* 81(3):536–545.
20. Lipp P, Niggli E (1993) Ratiometric confocal Ca(2+)-measurements with visible wavelength indicators in isolated cardiac myocytes. *Cell Calcium* 14(5):359–372.

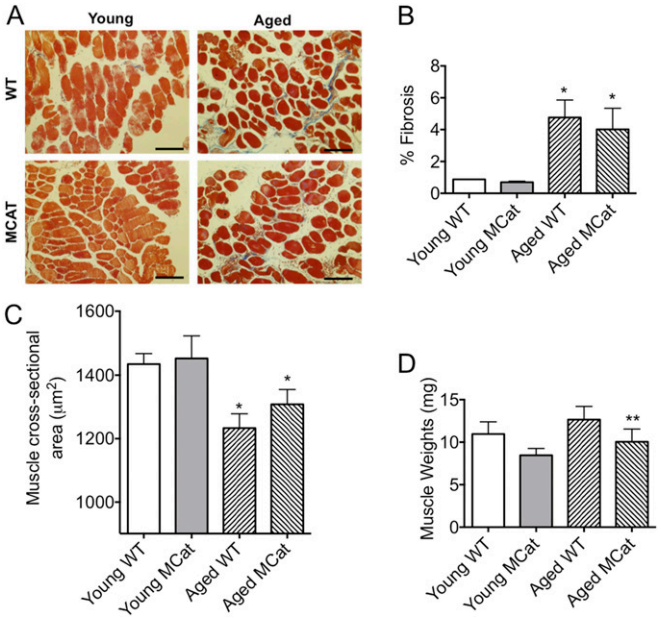

Fig. S1. MCat mice exhibit similar fibrosis levels, muscle fiber size and weight relative to age-matched WT. (*A*) Representative images showing skeletal muscle fibrosis using Masson's trichrome staining of tibialis anterior muscle. (Scale bar: 100 μm.) (*B*) Quantification of skeletal muscle fibrosis represented in *A*. (*C*) Muscle cross-sectional area (tibialis anterior muscle). (*D*) EDL muscle weights. Data are mean ± SEM (*$P < 0.05$ vs. young; **$P < 0.05$ vs. aged WT; ANOVA, Bonferroni post hoc test).

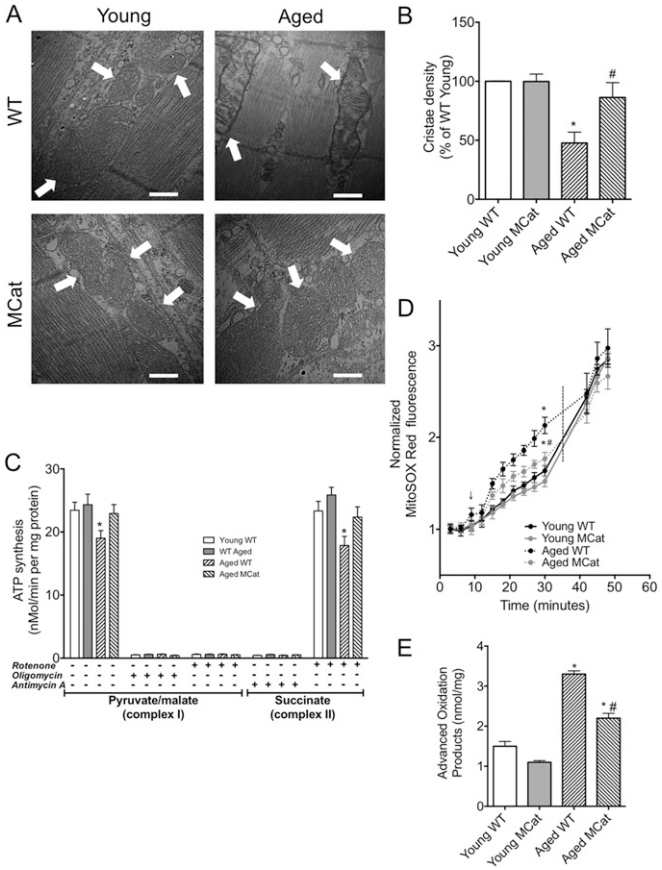

Fig. S2. Aged MCat mice exhibit enhanced mitochondrial structure and function and reduced skeletal muscle oxidation. (*A*) Representative images of the ultrastructure of tibialis anterior mitochondria from young and aged MCat and WT mice. (Magnification, 50,000×) (Scale bar: 500 nm). (*B*) Average cristae density, taken from images represented in *A*, $n > 3$ per group: (C) ATP production measured in presence of the indicated stimuli and inhibitors (*D*) Mitochondrial superoxide generation in FDB fibers. Arrow indicates the application of H_2O_2 (100 μM); dashed line indicates Antimycin A (10 μM), applied as positive control for superoxide production ($n = 6$ per group). (*E*) Advanced oxidation protein products (AOPP) as measured in skeletal muscle lysates. Data are mean ± SEM (*$P < 0.05$ vs. young WT, $^{\#}P < 0.05$ vs. aged WT; ANOVA, Bonferroni post hoc test, n = at least 3 per group).

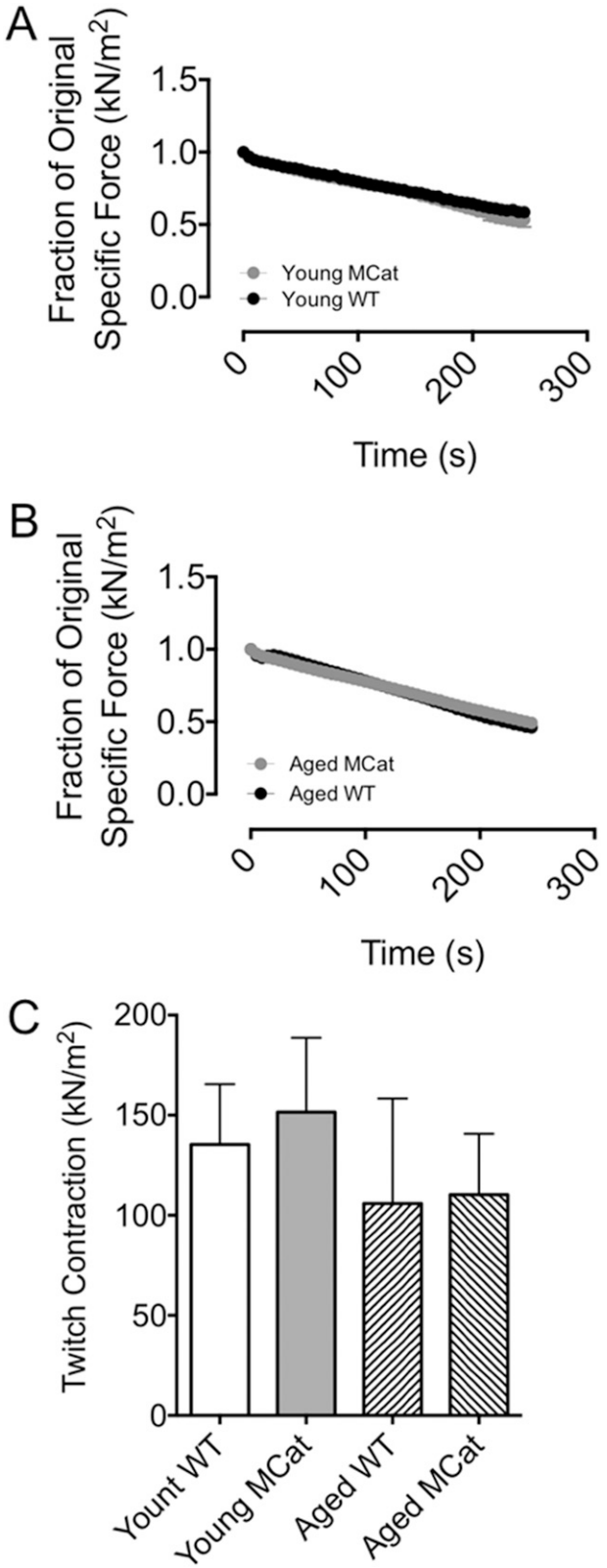

Fig. S3. MCat mice exhibit similar skeletal muscle fatigue and twitch contraction as WT age-matched littermates. (*A* and *B*) Skeletal muscle fatigue was achieved by repeatedly stimulating EDL muscles to tetanic contraction (70 Hz) and force was recorded (force was normalized to cross-sectional area and represented as fraction of the force at original tetanic stimulus; $n = 4–5$ for all groups). (*C*) EDL muscle twitch contraction (stimulated at 1 Hz; $n = 5–7$ for all groups).

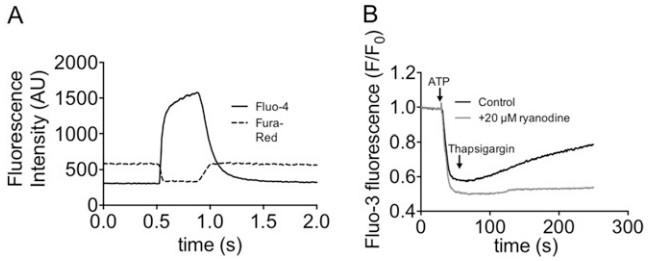

Fig. S4. Ratiometric measurement of SR Ca^{2+} load and RyR1 specificity of Ca^{2+} leak assay. (*A*) Representative traces of FDB muscle cells coloaded with Fluo-4 and Fura-Red in response to tetanic stimulation. (*B*) Representative trace depicting Ca^{2+} leak from SR microsomes in the presence or absence of the RyR1 specific drug, ryanodine.

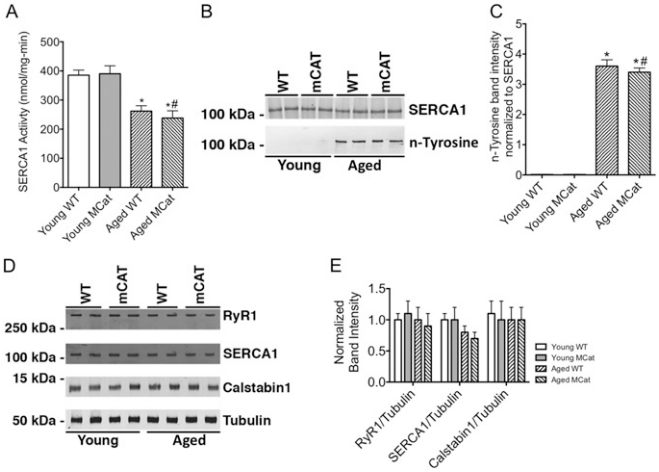

Fig. S5. SERCA activity in MCat mice is similar to WT. (*A*) SERCA1 activity in skeletal muscle. (*B*) Representative immunoblot from experiments of immunoprecipitated SERCA1 from murine skeletal muscle. (*C*) Bar graph showing quantification of the immunoblots in *B*. (*D*) Representative immunoblot using skeletal muscle lysates; (*E*) Bar graph showing quantification of the immunoblots in *D*. Data are mean ± SEM (*$P < 0.01$ vs. young WT, $^{\#}P < 0.01$ vs. young MCat, ANOVA).

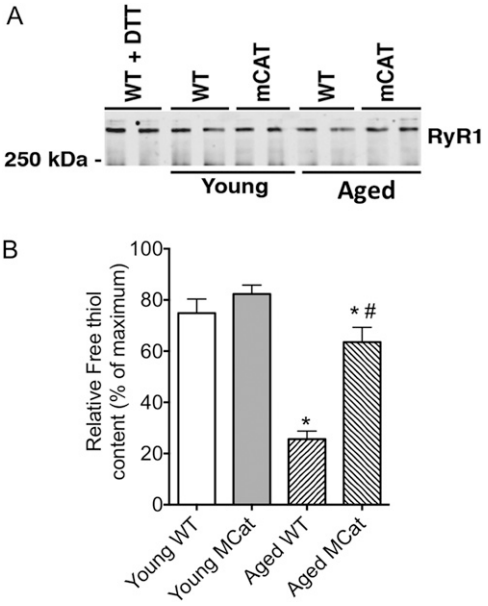

Fig. S6. Skeletal muscle from aged MCat mice exhibit increased free thiol content. (*A*) Representative immunoblot depicting RyR1 content in SR microsomes isolated from murine hind limb muscles. (*B*) Relative free thiol content in SR microsomes from murine hind limb muscles. Oxidation was normalized to maximum RyR1 thiol oxidation obtained with 10 mM DTT treatment of young WT SR. Data are mean ± SEM (*$P < 0.05$ vs. young WT, $^{\#}P < 0.05$ vs. aged WT; ANOVA).

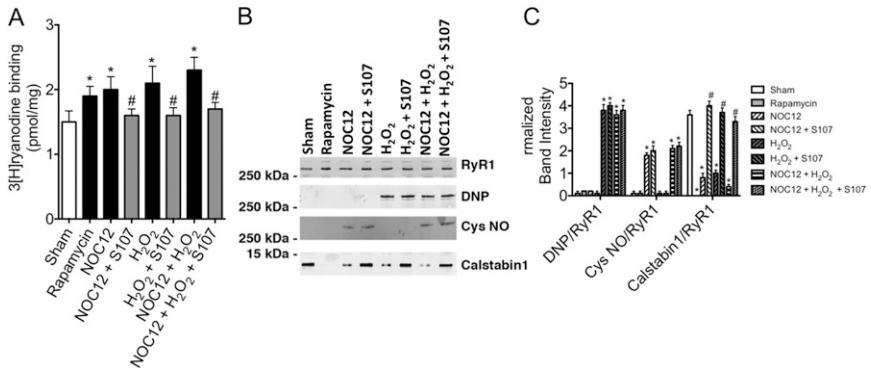

Fig. S7. RyR1 oxidation, nitrosylation, and calstabin1 depletion all independently affect RyR1 function. (*A*) Ryanodine binding assay performed on rabbit skeletal SR microsomes. (*B*) Representative immunoblot of immunoprecipitated RyR1 from rabbit skeletal SR microsomes, treated with indicated pharmacological agents. (*C*) Bar graph showing quantification of the immunoblots in *B*. Data are mean ± SEM (*$P < 0.05$ vs. sham, $^{\#}P < 0.05$ vs. that specific treatment, e.g., NOC12 or H_2O_2).